Combustion and Flame

Development and validation study of a 1D analytical model for the response of reheat flames to entropy waves

--Manuscript Draft--

Manuscript Number:	CNF-D-20-00402R2
Article Type:	Full Length Article
Keywords:	flame transfer function; non-linear flame response; entropy waves; reheat combustion; autoignition flames
Corresponding Author:	Francesco Gant Ansaldo Energia Switzerland Baden, SWITZERLAND
First Author:	Francesco Gant
Order of Authors:	Francesco Gant
	Andrea Gruber
	Mirko R. Bothien
Abstract:	Numerical simulations of laminar premixed flames burning hydrogen and methane in spontaneous ignition mode are performed by harmonically exciting the reactants' temperature at the domain inlet. The results are compared to an analytical model representing the same reactive flow configuration. The model provides a simplified but nevertheless accurate representation of reheat combustion taking place in sequential gas turbine combustors. An analytic expression for autoignition flames transfer functions to entropy waves is derived and used to extend transfer function models from the literature. For validation purposes, results from fully compressible Direct Numerical Simulations (DNS), including a complete representation of the fluctuating acoustic and entropic fields of the reactive flow, are analyzed and compared to incompressible Unsteady Reynolds-Averaged Navier-Stokes (URANS) simulations that only take into account the fluctuating entropic field. Methane flames are found to be more sensitive to entropic forcing than hydrogen flames, featuring nonlinear phenomena even for low excitation amplitudes. In the linear regime, all flames behave as predicted by the analytical model and the URANS simulations are found to correctly predict the fluctuating entropic field. The transition from linear to nonlinear flame response is described in detail and its physical mechanisms are explained. Comparisons with results available in the literature show good prediction capabilities, both in terms of flame describing function and integrated heat release rate. Limitations of the proposed analytical model with respect to real combustion systems are discussed and a simple correction is proposed.

This is the accepted version of an article publised in Combustion and Flame
http://dx.doi.org/10.1016/j.combustflame.2020.09.005

Development and validation study of a 1D analytical model for the response of reheat flames to entropy waves

Francesco Gant[a], Andrea Gruber[b,c], Mirko R. Bothien[a,d,*]

[a] *Ansaldo Energia Switzerland, Baden, Switzerland*
[b] *SINTEF Energy Research, Trondheim, Norway*
[c] *Department of Energy and Process Engineering, Norwegian University of Science and Technology, Trondheim, Norway*
[d] *Zürich University of Applied Sciences, Institute of Energy Systems and Fluid-Engineering, Winterthur, Switzerland*

Abstract

Numerical simulations of laminar premixed flames burning hydrogen and methane in spontaneous ignition mode are performed by harmonically exciting the reactants' temperature at the domain inlet. The results are compared to an analytical model representing the same reactive flow configuration. The model provides a simplified but nevertheless accurate representation of reheat combustion taking place in sequential gas turbine combustors. An analytic expression for autoignition flames transfer functions to entropy waves is derived and used to extend transfer function models from the literature. For validation purposes, results from fully compressible Direct Numerical Simulations (DNS), including a complete representation of the fluctuating acoustic and entropic fields of the reactive flow, are analyzed and compared to incompressible Unsteady Reynolds-Averaged Navier-Stokes (URANS) simulations that only take into account the fluctuating entropic field. Methane flames are found to be more sensitive to entropic forcing than hydrogen flames, featuring nonlinear phenomena even for low excitation amplitudes. In the linear regime, all flames behave as predicted by the analytical model and the URANS simulations are found to correctly predict the

*Corresponding author: Mirko Bothien
Email address: mirko.bothien@zhaw.ch (Mirko R. Bothien)

This is the accepted version of an article published in Combustion and Flame
http://dx.doi.org/10.1016/j.combustflame.2020.09.005

fluctuating entropic field. The transition from linear to nonlinear flame response is described in detail and its physical mechanisms are explained. Comparisons with results available in the literature show good prediction capabilities, both in terms of flame describing function and integrated heat release rate. Limitations of the proposed analytical model with respect to real combustion systems are discussed and a simple correction is proposed.

Keywords: flame transfer function, non-linear flame response, entropy waves, reheat combustion, autoignition flames

1. Introduction

In order to fulfill the goals of the Paris Agreement, it is expected that an increasing share of electric power will be generated from renewable energy sources (RES). Alongside renewables, only gas turbines are expected to also increase their share in the global energy mix [1]. In this context, where the power market is preferentially conditioned by unsteady generation by RES, longitudinally staged combustion systems seem to offer the most promising solution for today's power plants since they exhibit outstanding operational flexibility ensuring high turndown ratios, feature superior part-load efficiency, and can be operated on a wide range of different fuels (including hydrogen), while keeping pollutant emissions low [2]. A two-stage system, in which the first stage consists of a propagation-stabilized flame in a premix combustor and the second stage of a premix reheat flame, stabilized (mainly) by spontaneous ignition in a *sequential combustor*, is employed in the Ansaldo Energia GT36 H-class and GT26 F-class gas turbines [3, 4].

The interplay between these two different flame stabilization mechanisms allows to shift the fuel between the two combustors resulting in the above mentioned load flexibility and featuring hydrogen-firing capabilities presently unmatched by conventional single-stage systems [5]. The latter feature is a key advantage due to hydrogen's emerging relevance that equally applies, in a convenient synergy, to power generation schemes that produce hydrogen by re-

This is the accepted version of an article publised in Combustion and Flame
http://dx.doi.org/10.1016/j.combustflame.2020.09.005

forming of fossil fuels with carbon capture and storage (CCS) [6] or, exploiting excess power from non-dispatchable renewable energy resources (wind and solar), by water electrolysis in the context of large-scale energy storage solutions (power-to-H2-to-power) [7].

While advanced combustor staging, as implemented in the sequential combustor, has recently demonstrated outstanding hydrogen-firing capabilities of the reheat flame [5], conventional single-stage gas turbine combustors do not presently allow, without important compromises [8], for combustion of pure (undiluted) hydrogen due to issues with static and dynamic flame stability (i.e. avoiding flashback [9] and thermo-acoustics instabilities [10], respectively).

In this context, because of the crucial role played by the reheat combustion concept in today's and tomorrow's power generation, a number of experimental, numerical and analytical studies have been recently conducted to deepen the knowledge on the topic [5, 11, 12, 13]. One of the main differences with respect to single stage combustion systems is related to the reheat flame stabilization mechanism: depending on the used fuel or the respective load condition and associated first stage flame temperature, the importance of flame propagation relative to autoignition for the second stage flame stabilization can vary.

The autoignition and propagation regimes are very different. While propagating flames are dominated by convection-diffusion phenomena and characterized by velocities of the order of magnitude of $1-10\,\mathrm{m/s}$ [14], autoignition flames are convection-reaction dominated and stabilize even in flows characterized by very large velocities $u > 100\,\mathrm{m/s}$ [15].

In the current work we focus on purely autoignition stabilized combustion at relatively large flow velocities, relevant to gas turbine applications, at which aerodynamic conditions alone will not be sufficient to stabilize the flame. In this context, our goal is to study the flame response to external forcing. This is of fundamental importance in applications where one wants to assess the stability of the flame and often relies on flame transfer function (FTF) models [16] that describe the dynamic characteristics of the flame in a black box formulation. The FTF approach is not novel and has been extensively utilized both in aca-

This is the accepted version of an article publised in Combustion and Flame
http://dx.doi.org/10.1016/j.combustflame.2020.09.005

demic [17, 18] and industrial contexts [19] to build numerical surrogates of the flame and its interactions with the flow field. In [20] one can find examples of experimentally measured FTFs and how they can be used in network models. For propagation flames the aforementioned modelling strategy has become standard and analytical models have been developed to better understand the physics behind the problem, the famous Crocco $n-\tau$ interaction model [21] is an example.

In the context of autoignition flames, a number of numerical studies have been conducted in the recent past. Yang et al. [22] investigate the dynamic response of autoignition methane flames to axial velocity, equivalence ratio and temperature fluctuations using Large Eddy Simulations (LES). It is found that autoignition flames are predominantly sensitive to temperature fluctuations (and, to a minor extent, to equivalence ratio fluctuations). A quantification of the qualitative findings presented by Yang et al. [22] can be found in follow-up studies by Scarpato et al. [23] and later by Bothien et al. [24]: the key role of temperature fluctuations is verified by large FTF gains retrieved by the CFD/system identification procedure. The inclusion of compressibility in the model demonstrates that pressure fluctuations play a significant role and cannot be neglected. Physical insight in the nonlinear regime is given by Schulz and Noiray [25], who identify the appearance of local autoignition events upstream of the flame, first observed in experiments by DLR [11], as driving mechanism of the heat release unsteadiness. Indications from all these publications [22, 23, 24, 25] suggest that methane autoignition flames excited by temperature forcing respond with large heat release rate gains and early transition to nonlinearity.

Beyond the mentioned studies, which mostly focus on hydrocarbon fuels, only in a few works the characteristic features of hydrogen combustion at reheat conditions are investigated. In some of the earlier studies [11, 26, 27, 28], zero-dimensional (0D) or one-dimensional (1D) reactor simulations are performed to characterize ignition and propagation time scales. This is done in order to complement the planning and execution of full-scale, high-pressure experiments

This is the accepted version of an article publised in Combustion and Flame
http://dx.doi.org/10.1016/j.combustflame.2020.09.005

by theoretical considerations. Only very recently full-fledged, three-dimensional Direct Numerical Simulations (DNS) of turbulent premixed hydrogen-air combustion at reheat conditions (albeit atmospheric pressure) have been performed in conjunction with detailed chemical kinetics and Chemical Explosive Mode Analysis [29] to quantify the relative importance of flame propagation versus spontaneous ignition for a range of turbulence intensities in statistically planar flames [30] and in a semi-realistic combustor geometry [31].

The objective of this research is to gain analytical insight into the response of hydrogen and methane autoignition flames to forcing of the reactants' mixture temperature. Even if the sensitivity of autoignition flames to temperature fluctuations is more pronounced compared to pressure or velocity fluctuations [24, 25], no theoretical modeling of this phenomenon has been proposed so far. The present study aims at addressing the topic by complementing and extending the scope of previous investigations [12, 32, 33] so as to include inlet temperature fluctuations.

An analytical model first introduced by Zellhuber et al. [12] to study autoignition flame response to acoustic perturbations is extended to include temperature forcing in Sec. 3. It is used to get a better insight into the physics and understand the differences between methane and hydrogen. The analytical model is validated with respect to two significantly different numerical modelling approaches, a fully compressible Direct Numerical Simulation (Sec. 2.1) and an incompressible Unsteady Reynolds Averaged Navier-Stokes (URANS) simulation (Sec. 2.2). The two numerical methodologies are used to compare a highly-accurate, more computationally expensive model to a cheaper one, more suitable to numerical simulations of realistic geometries.

2. Numerical methods and configuration

In order to investigate the sensitivity of autoignition flames to entropic disturbances we perform two sets of 12 unsteady simulations on a simplified one-dimensional geometry. In the first set, a perfectly homogeneous mixture of

This is the accepted version of an article publised in Combustion and Flame
http://dx.doi.org/10.1016/j.combustflame.2020.09.005

vitiated-air and hydrogen at a fuel-air equivalence ratio $\phi = 0.35$ and $\bar{T} = 1100K$ is injected into the computational domain at a velocity of 200 m/s. This results in an autoignition delay time of $\tau \approx 0.12$ms (Cantera 0D, constant pressure reactor). For the second set, the fuel is methane at a fuel-air equivalence ratio $\phi = 0.515$ and $\bar{T} = 1450K$. The inlet velocity is decreased to 100 m/s and the ignition delay time becomes $\tau \approx 2.7$ms. The choice of the inlet temperature and velocity is to reduce the differences in autoignition delay times between the hydrogen and the methane mixtures. This is done with the constraint of remaining in gas-turbine relevant operating conditions (alas at atmospheric pressure) and in a regime of flame stabilization achieved purely by autoignition. The inlet temperature $T(x = 0, t)$ is forced sinusoidally at three different frequencies (f = 100, 500 and 1000 Hz) and four different perturbation amplitudes (ΔT = 2, 5, 10 and 25 K):

$$T(x = 0, t) = \bar{T} + \Delta T \sin(2\pi f t) \tag{1}$$

All computations in each set are performed twice, by means of compressible DNS (Sec. 2.1) and incompressible Unsteady URANS (Sec. 2.2) solvers. We utilize the same chemical kinetics mechanism in both simulation approaches, i.e. [34] for the hydrogen-air simulations and [35] for the methane-air ones.

2.1. Compressible DNS

Direct Numerical Simulations (DNS) of laminar premixed hydrogen flames at reheat conditions are performed using the S3D code [36] on 1D domains and constitute a validation base for the other models utilized herein. The DNS approach provides the most accurate representation of the unsteady reactive flows of interest but it is customarily limited to atmospheric pressure conditions due to the computational cost implied by its spatial and temporal resolution requirements.

The 1D physical domain represented in the DNS computations spans a length L_x = 30 cm (60 cm for the methane simulations) in the Cartesian x-direction. The Navier-Stokes equations for a reactive, multi-component, compressible fluid

This is the accepted version of an article publised in Combustion and Flame
http://dx.doi.org/10.1016/j.combustflame.2020.09.005

are discretized on a 30000-points (60000) Cartesian uniform mesh, providing a spatial resolution of 10μm, which is sufficient to accurately resolve the flame structure and all diffusive, reactive, and dissipative scales of the reacting flow. A mixture-averaged approximation is employed for the species diffusion coefficients that are formulated in terms of the binary diffusion coefficients and the mixture composition, where the binary coefficient matrix is symmetric and the diagonal elements are zero. Furthermore, thermal diffusion (the Soret effect) is included in the formulation for the species diffusion velocities because of its relevant role in mixtures containing hydrogen. A fourth-order-accurate, six-stages-explicit Runge-Kutta algorithm [37] is employed for time integration and the time step is fixed to 4 ns throughout the simulations. For additional details about the mathematical formulation see [36].

The 1D DNS simulations are initialized with a perfectly homogeneous mixture of vitiated-air and hydrogen (methane) characterized by a velocity of 200 m/s (100 m/s). This results in a residence time for the unburnt mixture t_{res} of $\sim$ 1.5 ms (6 ms). Sinusoidal forcing of the inlet temperature $T(x = 0, t)$ is started after a time period of 30 (120) ms (corresponding to 20 residence times t_{res}) in order to allow the initial acoustic transient (following ignition) to completely leave the computational domain.

For the domain inlet and outlet, acoustically non-reflective inflow and outflow boundary conditions, according to the NSCBC methodology adopted in S3D [36], are used. The NSCBC implementation in S3D is largely based on the formulation first described by Poinsot and Lele [38] and includes some modifications suggested later for the S3D code [39]. All DNS simulations are performed at atmospheric inlet pressures.

2.2. Incompressible URANS

The commercial software ANSYS Fluent v18.2 is deployed to perform the incompressible URANS simulations. The URANS modelling approach is computationally less expensive compared to the DNS one described in the previous section and it can be utilized to obtain predictions and indicative trends for

This is the accepted version of an article publised in Combustion and Flame
http://dx.doi.org/10.1016/j.combustflame.2020.09.005

reactive flows at high pressure conditions [24] and in complex geometries [23]. Additionally, it covers a wider range of parametric variations, alas at the cost of lower model accuracy.

The quasi 1D computational domain utilized in the URANS simulations consists of a two-dimensional straight duct measuring 30×2.5 cm (60×5 cm) in the longitudinal and transversal directions respectively. At the inlet, a constant velocity of 200 m/s (100 m/s) is imposed whereas the temperature is subject to sinusoidal forcing, Eq. (1). The reactants' composition at the domain inlet is kept constant and the fuel and oxidant are perfectly premixed. The mean pressure is imposed to atmospheric conditions at the domain outlet. The bottom and top walls are stationary perfectly adiabatic walls with zero shear stress. The structured mesh consists of $2.5 \cdot 10^5$ ($5 \cdot 10^5$) quadrilateral cells, refined at the flame location to better resolve the chemistry and the fluid dynamics. All transported quantities are discretized by a second order spatial and first order implicit temporal scheme and solved by a pressure-based transient solver. In order to represent these idealized, quasi-laminar flow conditions at high convection velocity, a very low turbulence intensity, with negligible effect on the turbulent (effective) dissipation, is imposed at the domain inlet of the URANS simulations. The choice of utilizing the present combination of URANS and combustion model instead of a purely laminar unsteady reactive flow model is motivated by the fact that the former is regularly applied to simulate turbulent reacting flows in realistic combustor geometries, as presented in [23, 40]. It is therefore convenient, in the present validation effort, to consistently include in the simulations homologous modelling features as far as it is practically feasible.

The combustion process in the URANS simulations is modeled with the method developed by Kulkarni and co-workers [41, 42] that relies on tabulated chemistry. Several earlier studies published in the literature [22, 23, 24] have already shown the model capability to accurately represent combustion dynamics of autoignition flames. Homogeneous reactor simulations are performed and the evolution of quantities of interest is stored. Additionally, a progress variable based on the sum of HO_2 and H_2O mass fractions [41] is defined and computed to

This is the accepted version of an article publised in Combustion and Flame
http://dx.doi.org/10.1016/j.combustflame.2020.09.005

parametrically map the flame structure. The transport equation of the mixture fraction and of the composite progress variable are solved and the quantities of interest are read from the homogeneous reactor tables. A more detailed explanation of the combustion modelling is available in [43]. The turbulence-chemistry interaction is represented by means of a composition transported FDF method based on an Eulerian formulation [42, 43].

3. Analytical model formulation

In this section an analytical model for autoignition flames response to temperature forcing is introduced. First, a note on entropy waves and indirect noise is given. Subsequently, the modeling hypotheses and the model description are explained.

3.1. Brief note on indirect noise

A brief discussion is opportune to clearly distinguish the objective of the present modelling effort from the entropy (indirect) noise framework [44]. As originally shown by Marble and Candel [45], hot spots and temperature fluctuations (i.e. entropy waves) generated by an unsteady combustion process and then convected downstream through a nozzle are able to generate acoustic waves. These acoustic waves, denoted as indirect noise, can travel back to the flame front and affect the combustion process, resulting in a feedback loop and generating thermo-acoustic instabilities [44]. The topic of indirect entropy noise has been the object of intensive study by different research groups [46, 47, 48, 49] and it is of great relevance in aero-engines applications. Therefore, it is important to clarify that our study does not deal with the effect of flame-generated entropy waves on the combustor thermoacoustics but focuses on the effect of incoming entropy waves on flame stabilization. This problem is usually of limited relevance in single-stage combustion systems because: (a) there is no physical mechanism that is able to generate appreciable entropy waves upstream of the flame itself and (b) premixed flames are not particularly sensitive to impinging

This is the accepted version of an article publised in Combustion and Flame
http://dx.doi.org/10.1016/j.combustflame.2020.09.005

entropy waves of modest amplitude. The situation is potentially very different in sequential combustion systems where: (a) the first-stage propagation-stabilized flame can produce non-negligible temperature fluctuations, i.e. entropy waves, in the products stream [50] and (b) the second-stage autoignition-stabilized flame is highly sensitive to these temperature fluctuations [40].

3.2. Model description

An idealized configuration, nominally identical to the DNS and URANS configurations, is considered to model the effects of entropy waves on the flame dynamics. It consists of a straight duct in which the fuel/air mixture entering the domain is treated as a series of plug flow reactors, see Fig. 1. The plug flow reactors are convected downstream by the mean flow and no interaction is considered among them. The time evolution of the chemical reactions in each plug flow reactor is independent from their time evolution in the other reactors. The advantage of this model lies in this hypothesis which is considered well-suited to tackle acoustic disturbances by Zellhuber [33]. As will become clear in Sec. 4, it is also appropriate in the vast majority of cases when dealing with entropy waves at the conditions studied here. As recently shown by Giusti [51], a model representation of diffusion, mixing and shear dispersion processes that arise from spatial variations of the mean velocity profile is necessary to correctly reproduce the attenuation of entropy fluctuations as they travel with the mean flow. However, none of these mechanisms is considered in the analytical model, as formulated in this section. In the current configuration and at the present reactive flow conditions, the very large velocities and the corresponding short traveling times between the inlet location and the flame stabilization position render the effects of the aforementioned physical processes negligible. These are typically characterized by longer time scales, in particular at lower frequencies. In the supplementary material we propose a simple correction to improve this approximation.

In steady-state conditions, an idealized reactor system, introduced into the domain at time t_i, is convected downstream by the mean flow $\bar{u}$ and ignites

This is the accepted version of an article publised in Combustion and Flame
http://dx.doi.org/10.1016/j.combustflame.2020.09.005

after a time $\bar{\tau}$, the autoignition delay time of the mixture initially present in the reactor system. The radical build-up experienced by the reactor system is governed by a normalized progress variable c, which spans the interval $[0, 1]$ from unburnt to burnt conditions; the progress variable temporal evolution will be affected by the reactor mean temperature and by acoustic fluctuations. With these hypotheses, the heat release rate can be expressed as (see [12]):

$$\dot{Q}(t) = \int_{-\infty}^{t} \Delta h_F \, \dot{m}_f(t_i) \, \dot{\omega}_c(t, t_i) dt_i \tag{2}$$

where Δh_F is the fuel lower heating value, $\dot{m}_f(t_i)$ is the fuel mass flow introduced at time t_i and $\dot{\omega}_c(t, t_i)$ is the source term associated to the progress variable c. Equation (2) is integrated, for a fixed time t, over all the reactors introduced into the computational domain, each indexed by its own injection time t_i and contributing to the overall heat release with its own reaction source term $\dot{\omega}_c(t, t_i)$ at the time t. The size of each reactor $\bar{u}dt_i$ becomes infinitesimal in Eq. (2).

In the current modelling framework, only two types of disturbances can affect the chemical reactions ongoing in each plug flow: entropic and acoustic disturbances (the effect of mixture fraction fluctuations is discussed in [52]). This is because no interactions are allowed between different plug flow reactors. These two disturbances are, in this idealized 1D model, independent of each other.

Acoustic disturbances are small variations of the local mean pressure and velocity fields, $p'(x, t) = p(x, t) - \bar{p}$ and $u'(x, t) = u(x, t) - \bar{u}$, respectively [16]. They differ substantially from entropic disturbances in that they travel both downstream and upstream with the speed of sound $\bar{c}$ with respect to the mean flow. The acoustic disturbances can be either described in terms of fluctuations in pressure $p'(x, t)$ and velocity $u'(x, t)$ or via the two travelling waves $f(x, t)$ and $g(x, t)$, the so called Riemann invariants [16], which are related to the primitive acoustic variables via a linear transform.

Entropic disturbances are small variations of the local mean entropic field $s'(x, t) = s(x, t) - \bar{s}$ and, after being generated or having entered the domain, are convected downstream by the mean flow $\bar{u}$ [51]. In the present configuration,

This is the accepted version of an article publised in Combustion and Flame
http://dx.doi.org/10.1016/j.combustflame.2020.09.005

entropic perturbations are artificially generated at the inlet and diffusion of entropy between adjacent plug flow reactor systems is neglected.

Since entropic disturbances travel with the mean flow velocity $\bar{u}$, each plug flow reactor is affected by a single associated entropic disturbance from the time of injection until it reaches the flame location. Differently, acoustic disturbances travel faster than the mean flow and are able to affect the chemical kinetics of multiple reactors.

In addition, two other fluid dynamics fields are usually of interest: the temperature field $T(x,t)$ and the density field $\rho(x,t)$. Assuming the ideal gas law to be valid, the linearized non-isentropic relations [14]

$$\frac{T'}{\bar{T}} = \frac{\gamma-1}{\gamma}\frac{s'}{R} + \frac{\gamma-1}{\gamma}\frac{p'}{\bar{p}} \tag{3a}$$

$$\frac{\rho'}{\bar{\rho}} = -\frac{\gamma-1}{\gamma}\frac{s'}{R} + \frac{1}{\gamma}\frac{p'}{\bar{p}} \tag{3b}$$

show the dependence of the temperature and pressure fields on the entropic and acoustic ones. In the following, we assume $p(x,t)$, $u(x,t)$ and $s(x,t)$ as independent field variables, whereas $T(x,t)$ and $\rho(x,t)$ are assumed to be dependent on the former ones.

Having defined the instantaneous integrated heat release rate $\dot{Q}(t)$ (Eq. (2)) and the three fundamental disturbances, $u'(x,t)$, $p'(x,t)$ and $s'(x,t)$, it is now appropriate to discuss how these perturbations affect the reaction chemistry. Two mechanisms are apparent from inspection of Eq. (2): the disturbances can alter the mass flow rate of fuel $\dot{m}_f$ and modify the temporal evolution of the source term $\dot{\omega}_c(t,t_i)$.

It is straightforward to obtain the (linearized) effect on the fuel mass flow rate:

$$\frac{\dot{m}'_f}{\bar{\dot{m}}_f} = \frac{u'}{\bar{u}} + \frac{\rho'}{\bar{\rho}} = \frac{u'}{\bar{u}} + \frac{1}{\gamma}\frac{p'}{\bar{p}} - \frac{\gamma-1}{\gamma}\frac{s'}{R} \tag{4}$$

where Eq. (3b) has been used and $\dot{m}_f$ has been rewritten as $\dot{m}_f = \bar{\dot{m}}_f + \dot{m}'_f$, $\bar{\dot{m}}_f$ being the constant mean value and $\dot{m}'_f$ its perturbation.

To model the effect of the disturbances on the source term $\dot{\omega}_c(t,t_i)$ the

This is the accepted version of an article published in Combustion and Flame
http://dx.doi.org/10.1016/j.combustflame.2020.09.005

following expression is adopted:

$$\dot{\omega}_c(t, t_i) = \bar{\dot{\omega}}_c(t - t_i) + \dot{\omega}'_c(t, t_i) + \tilde{\dot{\omega}}_c(t - t_i, t_i) \tag{5}$$

Assuming that the effects of acoustic and entropic disturbances on the flame can be linearly superposed, the source term $\dot{\omega}_c(t, t_i)$ can be separated in a constant part $\bar{\dot{\omega}}_c$, in a perturbation purely due to acoustic fluctuations $\dot{\omega}'_c(t, t_i)$ and in a perturbation purely due to entropic fluctuations $\tilde{\dot{\omega}}_c(t - t_i, t_i)$. In general, however, $\dot{\omega}'_c(t, t_i)$ and $\tilde{\dot{\omega}}_c(t - t_i, t_i)$ are nonlinear in their respective acoustic and entropic dependence.

The first term on the right-hand side of Eq. (5) is the source term of an unperturbed homogeneous 0D reactor at mean inlet pressure and temperature. In the absence of acoustic and entropic disturbances, this would be the only term present. The heat release rate given by this term at each time t does not depend on the time t itself but just on the residence time of the reactor in the domain $t - t_i \triangleq \Delta t_i$.

The term $\dot{\omega}'_c(t, t_i)$ results from acoustic disturbances. The isentropic pressure and velocity fluctuations tend to have a zero mean value (larger and smaller pressures will alternate), nevertheless they accumulate their effects over the plug residence time and can affect the heat release rate. Additionally, they can instantaneously change the pressure at the flame location and result in significant heat release rate fluctuations, especially for high frequencies. In contrast to the first two terms, they directly depend on the time t. For a more detailed discussion on this term, the reader is referred to Zellhuber *et al.* [12].

The term $\tilde{\dot{\omega}}_c(t - t_i, t_i)$ takes into account entropic disturbances. An entropic perturbation of the inlet temperature at time t_i results in a plug flow reactor with a modified heat release source term, where the heat release is anticipated/retarded with respect to the mean conditions for a hotter/colder mixture. This perturbation of the source term is a property of each reactor system and it is convected downstream with the reactor itself. The heat release rate depends just on the initial reactor time t_i and its residence time Δt_i.

Inserting the two contributions Eq. (4) and Eq. (5) into Eq. (2), neglecting

This is the accepted version of an article publised in Combustion and Flame
http://dx.doi.org/10.1016/j.combustflame.2020.09.005

second order terms, subtracting and dividing by the mean heat release $\bar{\dot{Q}} = \Delta h_F \bar{\dot{m}}_f$ we obtain:

$$\begin{aligned}\frac{\dot{Q}'(t)}{\bar{\dot{Q}}} &= \int_{-\infty}^{t} \left[\frac{\dot{m}'_f(t_i)}{\bar{\dot{m}}_f} \bar{\dot{\omega}}_c(\Delta t_i) + \dot{\omega}'_c(t,t_i) + \tilde{\dot{\omega}}_c(\Delta t_i, t_i) \right] dt_i \\ &= \int_{-\infty}^{t} \left[\left(\frac{u'(x_i,t_i)}{\bar{u}} + \frac{1}{\gamma}\frac{p'(x_i,t_i)}{\bar{p}} - \frac{\gamma-1}{\gamma}\frac{s'(x_i,t_i)}{R} \right) .. \right. \\ &\left. .. \bar{\dot{\omega}}_c(\Delta t_i) + \dot{\omega}'_c(t,t_i) + \tilde{\dot{\omega}}_c(\Delta t_i, t_i) \right] dt_i \end{aligned} \tag{6}$$

A convenient separation between terms of acoustic nature $\dot{Q}'_a(t)$ and entropic nature $\dot{Q}'_e(t)$ in Eq. (6) can be applied:

$$\frac{\dot{Q}'(t)}{\bar{\dot{Q}}} = \frac{\dot{Q}'_a(t)}{\bar{\dot{Q}}} + \frac{\dot{Q}'_e(t)}{\bar{\dot{Q}}} \tag{7a}$$

$$\frac{\dot{Q}'_a(t)}{\bar{\dot{Q}}} = \int_{-\infty}^{t} \left[\left(\frac{u'(x_i,t_i)}{\bar{u}} + \frac{1}{\gamma}\frac{p'(x_i,t_i)}{\bar{p}} \right) \bar{\dot{\omega}}_c(\Delta t_i) + \dot{\omega}'_c(t,t_i) \right] dt_i \tag{7b}$$

$$\frac{\dot{Q}'_e(t)}{\bar{\dot{Q}}} = \int_{-\infty}^{t} \left[-\frac{\gamma-1}{\gamma}\frac{s'(x_i,t_i)}{R} \bar{\dot{\omega}}_c(\Delta t_i) + \tilde{\dot{\omega}}_c(\Delta t_i, t_i) \right] dt_i \tag{7c}$$

3.3. A model for the source term

In order to derive an analytic expression for the flame transfer function due to entropy waves we introduce a model for the reaction source terms $\dot{\omega}_c(t,t_i)$ in Eq. (5):

$$\dot{\omega}_c(t,t_i) = \frac{1}{\sqrt{2\pi}}\frac{1}{\sigma} \exp\left[-\frac{1}{2} \left(\frac{t - t_i - \tau_0 e^{B(T_e(x_i,t_i)-\bar{T})} - \tau'(t_i)}{\sigma} \right)^2 \right] \tag{8}$$

where $T_e(x,t)$ is the entropic part of the temperature field and it is defined as $T_e(x,t) \triangleq \bar{T}(1 + (\gamma-1)s'(x,t)/(\gamma R))$ [1]. As commonly done in thermoacoustics, it is assumed that the heat release rate of a single plug flow reactor over its residence time $t - t_i$ has a Gaussian distribution with width σ around

[1] Equation (3a) allows for a straightforward definition of an entropic and acoustic temperature field: $T(x,t) = T_a(x,t) + T_e(x,t)$ where $T_a(x,t) \triangleq \bar{T}(\gamma-1)p'(x,t)/(\gamma\bar{p})$. Note how the mean temperature $\bar{T}$ is included in the entropic part $T_e(x,t)$

This is the accepted version of an article published in Combustion and Flame
http://dx.doi.org/10.1016/j.combustflame.2020.09.005

a mean ignition delay time $\tau = \tau_0 \exp\left[B(T_e(x_i,t_i) - \bar{T})\right]$. For a reactor system with mean inlet temperature $\bar{T}$, the mean ignition delay time will be τ_0, whereas for reactors affected by initial temperature perturbations the deviation from τ_0 will depend on the small negative constant B and on the small term τ'. Fluctuations in the entropic field are taken into account by the term $T_e(x_i,t_i) - \bar{T}$, whereas the effect of acoustic perturbations is embedded in the τ' term. As mentioned above, no coupling between the terms is considered. A detailed discussion about the significance of the term τ' is provided in [12, 33]. The exponential term $\tau_0 \exp\left[B(T_e(x_i,t_i) - \bar{T})\right]$ is obtained by fitting the mean autoignition delay time of an homogeneous reactor as function of different mean inlet temperatures, see Fig. 2. The parameters B, τ_0 and σ are obtained from Cantera 0D simulations and depend on the mean inlet pressure $\bar{p}$, temperature $\bar{T}$ and mixture composition. A physical interpretation is shown in Figs. 2 and 3.

From Eq. (5), with the ansatz Eq. (8) for the source term, an explicit formulation for $\bar{\dot{\omega}}_c(t-t_i)$, $\dot{\omega}'_c(t,t_i)$ and $\tilde{\dot{\omega}}_c(t-t_i,t_i)$ can be derived:

$$\bar{\dot{\omega}}_c(t-t_i) = \frac{1}{\sqrt{2\pi}}\frac{1}{\sigma}\exp\left[-\frac{1}{2}\left(\frac{t-t_i-\tau_0}{\sigma}\right)^2\right] \tag{9a}$$

$$\begin{aligned}\dot{\omega}'_c(t,t_i) &= \frac{1}{\sqrt{2\pi}}\frac{1}{\sigma}\exp\left[-\frac{1}{2}\left(\frac{t-t_i-\tau_0-\tau'(t_i)}{\sigma}\right)^2\right] - \bar{\dot{\omega}}_c(t,t_i) \\ &\approx \frac{1}{\sqrt{2\pi}}\frac{1}{\sigma}\exp\left[-\frac{1}{2}\left(\frac{t-t_i-\tau_0}{\sigma}\right)^2\right]\frac{t-t_i-\tau_0}{\sigma}\frac{1}{\sigma}\tau'(t_i)\end{aligned} \tag{9b}$$

$$\begin{aligned}\tilde{\dot{\omega}}_c(t-t_i,t_i) &= \frac{1}{\sqrt{2\pi}}\frac{1}{\sigma}\exp\left[-\frac{1}{2}\left(\frac{t-t_i-\tau_0 e^{B(T_e(x_i,t_i)-\bar{T})}}{\sigma}\right)^2\right] - \bar{\dot{\omega}}_c(t,t_i) \\ &\approx \frac{1}{\sqrt{2\pi}}\frac{1}{\sigma}\exp\left[-\frac{1}{2}\left(\frac{t-t_i-\tau_0}{\sigma}\right)^2\right]\frac{t-t_i-\tau_0}{\sigma}\frac{\tau_0}{\sigma}B(T_e(x_i,t_i)-\bar{T})\end{aligned} \tag{9c}$$

where the dependence of $\dot{\omega}'_c(t,t_i)$ on the acoustics is included in the term $\tau'(t_i)$ [12,33] and that of $\tilde{\dot{\omega}}_c(t-t_i,t_i)$ on entropic temperature fluctuations in $(T_e(x_i,t_i) - \bar{T})$.

This is the accepted version of an article published in Combustion and Flame
http://dx.doi.org/10.1016/j.combustflame.2020.09.005

3.4. Acoustic part

We consider the acoustic part of the unsteady normalized heat release $\dot{Q}'_a/\bar{\dot{Q}}$ as in Eq. (7b), substitute Eq. (9b) for the unsteady source term $\dot{\omega}'_c(t,t_i)$, integrate and transform in the frequency domain (all passages can be found explicitly in [33] or, alternatively, the same expression can be obtained under opportune assumptions on Eq. [34] in [12]):

$$\begin{aligned}\frac{\hat{\dot{Q}}'_a(\omega)}{\bar{\dot{Q}}} =& \left[\frac{\hat{u}'(x_i,\omega)}{\bar{u}} + \frac{1}{\gamma}\frac{\hat{p}'(x_i,\omega)}{\bar{p}}\right]\exp\left(-i\omega\tau_0\right)\exp\left(-\omega^2\sigma^2/2\right) + ... \\ &- \varphi_p\frac{\hat{p}'(x_i,\omega)}{\bar{p}}\exp\left(-i\omega\tau_0\right)\exp\left(-\omega^2\sigma^2/2\right) + ... \\ &+ \varphi_p\frac{\hat{p}'(\bar{x}_f,\omega)}{\bar{p}}\exp\left(-\omega^2\sigma^2/2\right) \end{aligned} \tag{10}$$

where $\bar{x}_f$ is the mean flame position and φ_p is a non-dimensional pressure sensitivity parameter obtained by comparing the source terms $\dot{\omega}_c$ of reactors evolving at different constant pressures $\bar{p}+p'$. The reader is referred to [12, 33] for a detailed definition and more complete description. The three terms contributing to the unsteadiness of the heat release reflect three different physical mechanisms. The first line of Eq. (10) represents the contribution given by a fuel mass flow rate modulation: the acoustics affect directly $\dot{m}_f$ (see Eq. (4)) and this results in a larger or smaller amount of fuel burnt. The second line of Eq. (10) corresponds to the cumulative effect of the alternation of positive and negative acoustic pressure on the plug flow. This effect is more pronounced at low frequencies and tends to become less prominent for higher frequencies, see [12]. The last term is a direct consequence of reaction sensitivity to the local pressure: the heat release is directly proportional to the pressure at the flame location. This contribution has been identified as crucial for the thermo-acoustic stability of the system at high frequencies [12].

3.5. Entropic part

We consider the entropic part of the unsteady normalized heat release $\dot{Q}'_e/\bar{\dot{Q}}$ as in Eq. (7c), substitute Eq. (9c) for the unsteady source term $\tilde{\dot{\omega}}_c(t,t_i)$, integrate

This is the accepted version of an article published in Combustion and Flame
http://dx.doi.org/10.1016/j.combustflame.2020.09.005

and transform in the frequency domain (all passages are detailed explicitly in the supplementary material):

$$\begin{aligned}\frac{\hat{\dot{Q}}'_e(\omega)}{\bar{\dot{Q}}} &= -\left(1+\tau_0 B\omega\bar{T}i\right)\exp\left(-i\omega\tau_0\right)\exp\left(-\omega^2\sigma^2/2\right)\frac{\hat{T}'_e(x_i,\omega)}{\bar{T}} \\ &= +\exp\left(-i\omega\tau_0\right)\exp\left(-\omega^2\sigma^2/2\right)\frac{\hat{\rho}'_e(x_i,\omega)}{\bar{\rho}} + ... \\ &\quad -\tau_0 B\omega\bar{T}i\,\exp\left(-i\omega\tau_0\right)\exp\left(-\omega^2\sigma^2/2\right)\frac{\hat{T}'_e(x_i,\omega)}{\bar{T}} \end{aligned} \tag{11}$$

where, in the last passage, the entropic part of the density fluctuations $\rho'_e/\bar{\rho} = -T'_e/\bar{T}$ has been introduced, as analogously already done for the temperature. The second line in Eq. (11) is particularly well-suited for a physical interpretation. Under the assumption of perfectly premixed fuel and gas, inlet density fluctuations (first term) result in larger amounts of fuel mass flow $\dot{m}_f$ and, therefore, increased heat release rates. The steady state source term $\bar{\dot{\omega}}_c(t-t_i)$ in Eq. (11) is indeed directly modulated by the density of the plug $\rho'_e/\bar{\rho} = -(\gamma-1)s'/(\gamma R)$. This term is analogous to the first term of Eq. (10) and together they fully capture the first term on the right hand side of Eq. (6). The second term of Eq. (11) is taking into account the effect of entropic temperature fluctuations, directly affecting the heat release term $\tilde{\dot{\omega}}_c(t-t_i,t_i)$. Physically, a larger/smaller inlet temperature modifies each reactor's chemical kinetics reducing/increasing the autoignition delay time. In contrast to the case of a modulation of density, each plug is still releasing the same amount of energy over its life time, however, its time evolution profile over the residence time Δt_i is different.

In Eq. (11), both density and temperature fluctuations are convected to the flame by the mean flow ($\exp\left(-i\omega\tau_0\right)$) and, for small delays $\omega\tau_0 << 1$, result in heat release rate fluctuations in phase with the density and in quadrature with respect to the temperature. At low frequencies the gain of the flame transfer function related to density fluctuations (second line of Eq. (11)) is constant ($\exp\left(-\omega^2\sigma^2/2\right) \approx 1$) whereas the temperature transfer function (third line) shows a linearly increasing gain with the frequency. In Sec. 4, it is shown that this quantity can reach large values, in particular for long ignition delay times

This is the accepted version of an article publised in Combustion and Flame
http://dx.doi.org/10.1016/j.combustflame.2020.09.005

τ_0.

3.6. Reheat flame transfer functions

We build the FTF of reheat flames to entropic and acoustic disturbances by merging Eq. (10) with Eq. (11):

$$\begin{aligned}\frac{\hat{\dot{Q}}'}{\bar{\dot{Q}}} =& \exp\left(-i\omega\tau_0\right)\exp\left(-\omega^2\sigma^2/2\right)\left[\frac{\hat{u}'(x_i,\omega)}{\bar{u}}+\frac{1}{\gamma}\frac{\hat{p}'(x_i,\omega)}{\bar{p}}\right]+...\\ &-\varphi_p\exp\left(-i\omega\tau_0\right)\exp\left(-\omega^2\sigma^2/2\right)\frac{\hat{p}'(x_i,\omega)}{\bar{p}}+...\\ &+\varphi_p\exp\left(-\omega^2\sigma^2/2\right)\frac{\hat{p}'(\bar{x}_f,\omega)}{\bar{p}}+...\\ &-\left(1+\tau_0 B\omega\bar{T}i\right)\exp\left(-i\omega\tau_0\right)\exp\left(-\omega^2\sigma^2/2\right)\frac{\hat{T}_e'(x_i,\omega)}{\bar{T}}\\ =&F_u\frac{\hat{u}'(x_i,\omega)}{\bar{u}}+F_p\frac{\hat{p}'(x_i,\omega)}{\bar{p}}+F_{T_e}\frac{\hat{T}_e'(x_i,\omega)}{\bar{T}}\\ =&\frac{\hat{\dot{Q}}_u'(\omega)}{\bar{\dot{Q}}}+\frac{\hat{\dot{Q}}_p'(\omega)}{\bar{\dot{Q}}}+\frac{\hat{\dot{Q}}_e'(\omega)}{\bar{\dot{Q}}}\end{aligned} \tag{12}$$

Here, we introduce the flame transfer functions F_u, F_p, F_{T_e} and decompose the acoustic part of the unsteady heat release in its velocity and pressure components $\dot{Q}_a' = \dot{Q}_p' + \dot{Q}_u'$. Additionally, notice that it is necessary to express the acoustic pressure at the mean flame location $p'(\bar{x}_f)$ as function of the pressure at the inlet; this requires an additional hypothesis, for example the knowledge of the acoustic impedance at the inlet.

4. Results

The unsteady fluctuations of temperature, pressure, velocity and density at the inlet and of the overall integrated heat release rate in the domain are extracted from the simulations introduced in Sec. 2 and the results are compared to the analytic results derived in Sec. 3.

4.1. Hydrogen flames

Figure 4 shows two periods of unsteady normalized heat release rate, extracted from DNS and URANS simulations of a hydrogen flame (forcing at

This is the accepted version of an article publised in Combustion and Flame
http://dx.doi.org/10.1016/j.combustflame.2020.09.005

100 Hz and 2 K). The continuous lines are the analytical results from Eq. (12). Among the three contributions to the overall heat release rate, $\dot{Q}'_e(t)$, $\dot{Q}'_u(t)$ and $\dot{Q}'_p(t)$, none is dominant and their sum (purple line) closely follows the DNS results (green crosses), hence validating the model. The URANS integrated heat release rate (blue circles) shows a significant mismatch with the DNS. This is due to the incompressible nature of the URANS simulations that do not account for the acoustic contributions. Interestingly, URANS results perfectly match the entropic part of the heat release rate, $\dot{Q}'_e(t)/\bar{\dot{Q}}$.

The excellent match observed in Fig. 4 is verified also over all remaining 11 simulations. Figure 5 shows the identified gains and phases of the heat release rate for the two sets of hydrogen simulations, URANS and DNS (red and blue symbols respectively). The red line represents the entropic contribution to the heat release rate, $\hat{\dot{Q}}'_e/\bar{\dot{Q}}$, i.e., the last term on the right hand side of Eq. (12). The blue line is the overall $\hat{\dot{Q}}'/\bar{\dot{Q}}$ in Eq. (12). The gain is normalized with the entropic part of the inlet temperature fluctuation, $|\hat{T}'_e(x_i,\omega)/\bar{T}|$. Increasing the forcing amplitude simulations at the same frequency only slightly changes the results. This suggests that all simulations fall in the linear regime and it has been verified by checking that the power content of the heat release signal at frequencies other than the excited one is negligible. Additionally, the purely linear transfer function of Eq. (12), blue line, perfectly reproduces the phenomenon at the three frequencies investigated, confirming the linearity assumption. With respect to the URANS simulation, the mismatch observed in Fig. 4 is observable for all results, especially in the phase. The red line, $\hat{\dot{Q}}'_e/\bar{\dot{Q}}$ of Eq. (12), confirms that incompressible URANS simulations excited by entropy waves are correctly reproduced by Eq. (11).

4.2. Methane flames

We repeat the analysis performed in Sec. 4.1 for the methane flames. In Fig. 6, we plot gains and phases of the normalized heat release rate and we

This is the accepted version of an article publised in Combustion and Flame
http://dx.doi.org/10.1016/j.combustflame.2020.09.005

compare them with Eq. (12) [2]. With respect to the hydrogen case depicted in Fig. 5 several differences can be observed. Firstly, the gains are an order of magnitude larger if methane is used as fuel. This is a consequence of the different autoignition delay times, which are for methane, at the investigated conditions, more than 10 times larger than for hydrogen. Therefore, τ_0 in Eq. (11) is 10 times larger and so are the resulting gains. This is a general conclusion for the autoignition flames studied in this work: *large ignition delay times produce large gains* (see also Fig. 7). Furthermore, some of the numerical simulations (at 10 and 25 K amplitudes, both for DNS and URANS) feature reduced gains with respect to the model, showing clear nonlinearities, i.e. the heat release rate responds significantly at higher harmonics of the forcing frequency. As expected, this phenomenon is observed for large amplitude excitation at the inlet, but also at high frequencies, i.e., the linearity of the flame response is frequency dependent. We discuss the nonlinear regime in Sec. 4.4. Additionally, it is remarkable that hydrogen flames, as opposed to methane flames, respond linearly for the considered cases. This can be explained by the fact that hydrogen is already very reactive compared to methane and its reactivity is significantly less modified than methane for the same excitation amplitude, see again Sec. 4.4. Looking at the purely entropic contribution (red line) and at the URANS simulations we notice a decrease of gains for frequencies larger than $f \approx 700$ Hz, even if the gain of Eq. (11) contains a direct ω term. Two factors are responsible for this: high frequencies disturbances are affected by the low-pass behaviour of the term $\exp\left[-(\omega^2\sigma^2)/2\right] \leq 1$ and diffusive processes upstream of the flame smoothen flow inhomogeneities. For the interested reader, we discuss in detail this effect in the supplementary material. With respect to the phase, it can be concluded that it is not significantly affected by the nonlinearities.

In Fig. 7, the transfer functions F_{T_e}, F_p and F_u defined in Eq. (12) are

[2] The evaluation of $\hat{\dot{Q}}'/\bar{\dot{Q}}$ requires the knowledge of the quantities $\hat{u}'(x_i,\omega)$, $\hat{p}'(x_i,\omega)$ and $\hat{T}'(x_i,\omega)$ at the inlet at each frequency ω. We extrapolated these values from the simulations with $\Delta T = 2\,\mathrm{K}$, performing two additional simulations at $f = 300\,\mathrm{Hz}$ and $f = 700\,\mathrm{Hz}$.

This is the accepted version of an article publised in Combustion and Flame
http://dx.doi.org/10.1016/j.combustflame.2020.09.005

plotted. Interestingly, the observed gains are much larger for the methane case than for the hydrogen one, which is in line with the observations made for the simulations. The gain of the F_{T_e} transfer function is proportional to the mean inlet temperature $\bar{T}$ and the mean ignition delay time τ_0, Eq. (11); both terms are larger for the methane flame considered and this explains the resulting larger gains. For both fuels, the entropic contribution dominates with respect to the ones for pressure and velocity. This is an artifact of the simplified geometry: for more complex setups turbulence and mixing processes smoothen temperature inhomogeneities before reaching the flame, especially at high frequencies. From the phase plot, the difference between ignition delay time for the two fuels is evident. For methane the phase slope is much steeper corresponding to the lower reactivity.

4.3. Comparison with findings from the literature

In this section we report the main findings on autoignition flames FTFs and compare them with results from three studies available in the literature: Bothien et al. [24] (compressible LES on a simplified 3D model of a sequential combustor, at gas turbine relevant temperatures and pressures), Schulz and Noiray [25] (compressible LES of a backward facing step modeling a sequential combustor) and Scarpato et al. [23] (high pressure compressible LES with broadband inlet excitation coupled with system identification [53] of a gas turbine sequential burner). Following phenomena are observed:

- At low frequencies, the FTF gains for temperature fluctuations are linearly increasing with the excitation frequency (Fig. 9 in [24], right plot of Fig. 1 in [25], Fig. 7 in [23]) .
- Pressure and velocity fluctuations play a minor role when compared to temperature fluctuations (Fig. 9 in [24], Fig. 7 in [23]).
- Temperature FTFs show very large gains ($\approx$ 5-50), with larger values typical of simplified geometries (present work, [24]) and smaller ones observed for more complex geometries and/or highly turbulent conditions [23, 25].

This is the accepted version of an article publised in Combustion and Flame
http://dx.doi.org/10.1016/j.combustflame.2020.09.005

- More complex geometries require a larger amplitude of the excitation at the inlet in order to perturb the flame ($\Delta T/\bar{T} = 0.35\%$ in the present work for a CH4 flame excited at 5K , 0.76% in [24], 2.4% in [25], 4.7% in [23]). This highlights the significant effect of dispersion, mixing and turbulence in real geometries.

- Transition to a nonlinear flame response can happen already at low excitation amplitudes and is frequency dependent (see Fig. 6, Sec. 4.4 in the present work and Fig. 12 in [24]).

To the knowledge of the authors, so far no FTF measurements for autoignition flames have been conducted which is most likely due to the fact that the flame dynamics strongly depend on the mean pressure level and FTF measurements at high pressure are not straightforward and involve high costs [24] .

4.4. From linear to nonlinear regime

Recent research efforts [24, 25, 40] have addressed the effect of an increase in excitation amplitude on the flame response. In this section, a description of the transition from linear to nonlinear response is given based on 1D simulations. To this end we consider the four DNS simulations of methane at a forcing frequency of $f = 500\,\mathrm{Hz}$. These conditions are chosen because they feature a smooth transition from the linear to highly nonlinear regime. We present the results for each forcing amplitude ΔT in a different frame in Fig. 8. In particular, frames a),b),c) and d) correspond to $\Delta T = 2\,\mathrm{K}$, $\Delta T = 5\,\mathrm{K}$, $\Delta T = 10\,\mathrm{K}$ and $\Delta T = 25\,\mathrm{K}$, respectively. All four frames are organized in the same fashion: on the top we present the temperature field over the full length of the domain ($x = 0 - 60$ cm) and over three inlet excitation periods ($1/f = 2\,\mathrm{ms}$). On the bottom, three different scalar quantities are reported for the same corresponding time span: in red the normalized inlet temperature $T'(x = 0, t)/\bar{T}$, in continuous blue the spatially-integrated normalized heat release rate $\dot{Q}'(t)/\bar{\dot{Q}}$ and in dashed blue the analytically-computed $\dot{Q}'_e(t)/\bar{\dot{Q}}$. This last term has been obtained by numerical integration of the source term $\tilde{\dot{\omega}}_c(t, t_i)$ as presented in the first line of Eq. (9c).

This is the accepted version of an article publised in Combustion and Flame
http://dx.doi.org/10.1016/j.combustflame.2020.09.005

We start from the smallest excitation amplitude, $\Delta T = 2\,\mathrm{K}$ in Fig. 8 (a). At this excitation amplitude the flame responds linearly (the integrated heat release is a sinusoidal curve) and the flame is oscillating slowly and symmetrically with respect to the mean flame position $\bar{x}_f = \bar{u}\tau_0 \approx 27$ cm. In particular, the hot and cold spots introduced at the inlet impinge alternately on the flame, which moves forward when the mixture is more reactive (hot spots) and backwards when it is less reactive (cold spots). Note also that the entropic contribution to the unsteady heat release rate $\dot{Q}'_e(t)/\bar{\dot{Q}}$ (dashed blue line) is not representing the overall heat release rate $\dot{Q}'(t)/\bar{\dot{Q}}$ (continuous blue line) due to the fact that the acoustics $\dot{Q}'_a(t)/\bar{\dot{Q}}$ are playing a non-negligible role (dotted blue line). This is comparable to the findings presented in Fig. 4.

At higher excitation amplitudes, $\Delta T = 5\,\mathrm{K}$ in Fig. 8 (b), asymmetries start to arise. In particular, we notice that the flame spends 58% of a period moving backwards, burning less fuel (negative $\dot{Q}'(t)$), and just 42% moving forward. In this 42% of the time the flame moves upstream and a large amount of fuel is burn. This corresponds to the larger amplitude of the positive peaks of the continuous blue line $\dot{Q}'(t)/\bar{\dot{Q}}$ in contrast to the smaller amplitude of the negative peaks. The reason for the asymmetry is the exponential dependence of the autoignition delay time τ on the temperature, see Fig. 2. Due to this, negative ΔT result in ignition delay time variations which are larger than those resulting from a positive ΔT.

In Fig. 8 (c) results for $\Delta T = 10\,\mathrm{K}$ are shown. The trend observed for 5 K is amplified. In particular, approximately 66% of the time the flame is moving backwards and the forward jump happens so rapidly that it results in a spike in the heat release time trace. In this short time interval, a large amount of fuel is burnt because the relative velocity between the flame front and the mean flow is suddenly increased.

Figure 8 (d) illustrates the results for very large forcing amplitude, namely $\Delta T = 25\,\mathrm{K}$. When a cold spot is injected at the domain inlet (A) it is convected downstream and when impinging on the flame, the flame front is moved downstream (B arrow). During this motion the relative velocity between the flame

This is the accepted version of an article publised in Combustion and Flame
http://dx.doi.org/10.1016/j.combustflame.2020.09.005

and the fluid is reduced, a smaller amount of fuel is burnt and consequently $\dot{Q}'(t)$ is negative. In the meantime, a hot spot has entered the domain and, given its higher reactivity, spontaneously autoignites (C). The new flame front (C) generates an acoustic wave (D) traveling back to the domain inlet with the speed of sound. Upstream and downstream of the flame front (C) fresh unburnt gases are present. The flame front splits in two separate fronts (E), one moving upstream and the other downstream. In this very moment three flame fronts exist and this reflects into a peak in the heat release rate. When the downstream-moving flame front (E) meets the original flame front (B) the two merge in (F). The result is an acoustic wave traveling downstream at the speed of sound (G) and combustion products convected to the outlet by the mean flow (H).

The appearance of multiple flame fronts in similar conditions has already been observed in LES and analytical models of autoignition flames and is documented in a previous work [40]. The present results confirm the observed phenomenon, for the first time, by highly accurate DNS calculations. It corresponds to the appearance of autoignition kernels in the burner mixing section of more complex geometries [25]. This has been observed experimentally [11, 50] and numerically [25, 31, 40] and has been explained as an effect of either hot spots [25, 40] or acoustic interference patterns [31]. The effect on the flame dynamics is of relevance both in case of an autoignition stabilized flames [40] and in case of a propagation-stabilized ones [25].

To conclude this section, a plot of the nonlinear flame transfer function (commonly referred to as flame describing function) to entropy fluctuations at an excitation frequency of 500 Hz is presented in Fig. 9 . The top plot presents the amplitude of the entropic part of the normalized heat release rate, $|\hat{\dot{Q}}'_e/\bar{\dot{Q}}|$, the middle and bottom plots the gain and phase of the flame describing function $FDF(\omega)$, respectively:

$$FDF(\omega) \triangleq \frac{\hat{\dot{Q}}'_e/\bar{\dot{Q}}}{\hat{T}_e{}'/\bar{T}} \tag{13}$$

The yellow curve is obtained, by numerical integration of the source term

This is the accepted version of an article publised in Combustion and Flame
http://dx.doi.org/10.1016/j.combustflame.2020.09.005

$\tilde{\omega}_c(t, t_i)$ in Eq. (9c) resulting in the unsteady heat release rate $\dot{Q}(t)$. This quantity is then normalized, $\dot{Q}'(t)/\bar{\dot{Q}}$ and its amplitude and phase are extracted at the fundamental frequency f = 500 Hz. The blue and red curves are derived from post-processing DNS and URANS data, respectively. The very large gains in the limit of excitation amplitude 0 drop significantly as the forcing amplitude is increased. This is related to the highly nonlinear phenomena (Fig. 8, frames (c) and (d)), which result in a nonlinear system response at different frequencies from the fundamental one. An analytic rule-of-thumb estimate for the forcing amplitude ΔT_{NL} for which an autoignition flame starts to respond nonlinearly is:

$$\Delta T_{NL} = -\frac{1}{5B}(4\omega^2\tau_0^2 + 1)^{-1/2} \exp\left(3\,\omega^2\sigma^2/2\right) \tag{14}$$

Equation (14) has been obtained by expansion of the source term $\tilde{\omega}_c(t, t_i)$ in Eq. (9c) to the second order in the forcing amplitude $T_e - \bar{T}$ and setting the ratio between the second and the first harmonic amplitude to 1/10. More details can be found in the supplementary material. The value of the critical excitation amplitude ΔT_{NL} for the case reported in Fig. 9 and derived with Eq. (14) is 2.2 K ($|T_e'/\bar{T}| \approx 0.15\%$). This means that already the 2 K simulation is at the limit of linearity. Comparing Fig. 9 with similar plots available in literature, similarities with results reported by Bothien et al. [24] can be observed, where the onset of nonlinearities was found at $|T'/\bar{T}| \approx 2\%$. The difference in magnitude could be due to different operating conditions ($\bar{T}$, $\bar{p}$), different forcing frequency and turbulent and mixing phenomena inherent to the 3D geometrical configuration. Interestingly, Schulz and Noiray [25], find that the onset of nonlinearity due to flame saturation is characterized by an increase of the gain with the forcing amplitude. This is in contrast to both Fig. 9 and different cases in literature [54, 55]. In the authors' opinion an explanation for this mismatch is to be found in the different flame stabilization mechanism: the flame in [25] is propagating whereas the flame in Fig. 9 is purely autoignition driven. The onset of a nonlinear behaviour is at $|T_e'/\bar{T}| \approx 2.5\%$, similarly to the observations in [24].

This is the accepted version of an article published in Combustion and Flame
http://dx.doi.org/10.1016/j.combustflame.2020.09.005

5. Conclusions

In this work, DNS and URANS calculations of premixed hydrogen and methane flames at reheat conditions subject to inlet temperature fluctuations are performed. First, results from the two numerical approaches are compared to each other, assessing the ability of URANS simulations based on tabulated chemistry to capture the entropic contribution to the unsteady heat release. This is an important benchmark for numerical simulations at gas turbine-relevant operating conditions, i.e., high pressure and preheat temperature, where the geometrical complexity and extension of the computational domain renders high-resolution DNS unfeasible and URANS/LES based on tabulated chemistry represent the only viable numerical modelling approaches.

Furthermore, an analytic model of the flame dynamics is proposed extending previous work [12] by including the important effect of entropic forcing. It is analytically proven that reheat flames exhibit very large gains, linearly increasing with excitation frequency. This result is in line with numerical results shown in previous works [22, 24] and provides greater insight into the underlying physical mechanisms. The capability of the model to reproduce high-accuracy DNS data is demonstrated. Significant differences between hydrogen and methane flames are revealed. In particular, the larger ignition delay times of methane flames appear to be responsible for increased gains and early transition to nonlinearities.

The physical phenomenon responsible for the onset of a nonlinear flame response is found to be the modulation of autoignition delay time of the unburnt mixture. DNS results fully validate the proposed explanation and confirm the validity of the analytical model for nonlinear studies. In order to take into account the effects of mixing, dispersion and turbulence, a simple diffusion transfer function is proposed in the supplementary material as a tool for modeling more complex geometries.

This is the accepted version of an article publised in Combustion and Flame
http://dx.doi.org/10.1016/j.combustflame.2020.09.005

Acknowledgments

This publication has been produced with support from the NCCS Centre, performed under the Norwegian research program Centres for Environment-friendly Energy Research (FME). The authors acknowledge the following partners for their contributions: Aker Solutions, ANSALDO Energia, CoorsTek Membrane Sciences, Gassco, KROHNE, Larvik Shipping, Norcem, Norwegian Oil and Gas, Quad Geometrics, Shell, Statoil, TOTAL, and the Research Council of Norway (257579/E20). The computational allocation for the present study was provided by NERSC - the National Energy Research Scientific Computing Center in the United States - and by UNINETT Sigma2 - the National Infrastructure for High Performance Computing and Data Storage in Norway (project number nn9527k).

This project has received funding from the European Union's Horizon 2020 research and innovation programme under the Marie Sklodowska-Curie grant agreement No. 765998 , ANNULIGhT.

References

[1] IEA, World Energy Outlook 2018, Tech. rep., Paris (2018).
URL //www.iea.org/reports/world-energy-outlook-2018

[2] A. Ciani, M. Bothien, B. Bunkute, J. Wood, G. Früchtel, Superior fuel and operational flexibility of sequential combustion in Ansaldo Energia gas turbines, Journal of the Global Power and Propulsion Society 3 (2019) 1–16. doi:10.33737/jgpps/110717.
URL http://www.journalssystem.com/jgpps/,110717,0,2.html

[3] D. A. Pennell, M. R. Bothien, A. Ciani, V. Granet, G. Singla, S. Thorpe, A. Wickstroem, K. Oumejjoud, M. Yaquinto, An Introduction to the Ansaldo GT36 Constant Pressure Sequential Combustor, in: Volume 4B: Combustion, Fuels and Emissions, Paper No. GT2017-64790, ASME, Charlotte, North Carolina, USA, 2017. doi:10.1115/GT2017-64790.

URL http://proceedings.asmedigitalcollection.asme.org/proceeding.aspx?doi=10.1115/GT2017-64790

[4] F. Güthe, J. Hellat, P. Flohr, The Reheat Concept: The Proven Pathway to Ultralow Emissions and High Efficiency and Flexibility, Journal of Engineering for Gas Turbines and Power 131 (2) (2009) 021503. doi:10.1115/1.2836613.
URL http://GasTurbinesPower.asmedigitalcollection.asme.org/article.aspx?articleid=1474556

[5] M. R. Bothien, A. Ciani, J. P. Wood, G. Fruechtel, Toward Decarbonized Power Generation With Gas Turbines by Using Sequential Combustion for Burning Hydrogen, Journal of Engineering for Gas Turbines and Power 141 (12) (2019) 121013. doi:10.1115/1.4045256.
URL https://asmedigitalcollection.asme.org/gasturbinespower/article/doi/10.1115/1.4045256/1065885/Toward-Decarbonized-Power-Generation-With-Gas

[6] G. Collidi, Reference data and supporting literature reviews for smr based hydrogen production with ccs, Tech. Rep. Tech.Rep. 2017-TR3, IEAGHG (2017).
URL https://ieaghg.org/publications/technical-reports

[7] M. Kloess, K. Zach, Bulk electricity storage technologies for load-leveling operation – An economic assessment for the Austrian and German power market, International Journal of Electrical Power & Energy Systems 59 (2014) 111–122. doi:10.1016/j.ijepes.2014.02.002.
URL https://linkinghub.elsevier.com/retrieve/pii/S0142061514000544

[8] P. Chiesa, G. Lozza, L. Mazzocchi, Using Hydrogen as Gas Turbine Fuel, Journal of Engineering for Gas Turbines and Power 127 (1) (2005) 73–80. doi:10.1115/1.1787513.

This is the accepted version of an article pulished in Combustion and Flame
http://dx.doi.org/10.1016/j.combustflame.2020.09.005

URL https://asmedigitalcollection.asme.org/gasturbinespower/article/127/1/73/461864/Using-Hydrogen-as-Gas-Turbine-Fuel

[9] J. Fritz, M. Kröner, T. Sattelmayer, Flashback in a Swirl Burner With Cylindrical Premixing Zone, Journal of Engineering for Gas Turbines and Power 126 (2) (2004) 276–283. doi:10.1115/1.1473155.
URL https://asmedigitalcollection.asme.org/gasturbinespower/article/126/2/276/461764/Flashback-in-a-Swirl-Burner-With-Cylindrical

[10] T. C. Lieuwen, V. Yang, Combustion Instabilities In Gas Turbine Engines: Operational Experience, Fundamental Mechanisms, and Modeling, American Institute of Aeronautics and Astronautics, Reston ,VA, 2006. doi:10.2514/4.866807.
URL http://arc.aiaa.org/doi/book/10.2514/4.866807

[11] J. M. Fleck, P. Griebel, A. M. Steinberg, C. M. Arndt, C. Naumann, M. Aigner, Autoignition of hydrogen/nitrogen jets in vitiated air crossflows at different pressures, Proceedings of the Combustion Institute 34 (2) (2013) 3185–3192. doi:10.1016/j.proci.2012.05.039.
URL https://linkinghub.elsevier.com/retrieve/pii/S1540748912000405

[12] M. Zellhuber, B. Schuermans, W. Polifke, Impact of acoustic pressure on autoignition and heat release, Combustion Theory and Modelling 18 (1) (2014) 1–31. doi:10.1080/13647830.2013.817609.
URL http://www.tandfonline.com/doi/abs/10.1080/13647830.2013.817609

[13] O. Schulz, N. Noiray, Combustion regimes in sequential combustors: Flame propagation and autoignition at elevated temperature and pressure, Combustion and Flame 205 (2019) 253–268. doi:10.1016/j.combustflame.2019.03.014.

URL https://linkinghub.elsevier.com/retrieve/pii/S0010218019301087

[14] R. J. Kee, M. E. Coltrin, P. Glarborg, H. Zhu, Chemically Reacting Flow: Theory, Modeling, and Simulation, Wiley, 2017. doi:10.1002/9781119186304.
URL http://doi.wiley.com/10.1002/9781119186304

[15] A. Krisman, E. R. Hawkes, J. H. Chen, The structure and propagation of laminar flames under autoignitive conditions, Combustion and Flame 188 (2018) 399–411. doi:10.1016/j.combustflame.2017.09.012.
URL https://linkinghub.elsevier.com/retrieve/pii/S0010218017303425

[16] T. C. Lieuwen, Unsteady combustor physics, Cambridge University Press, 2013.
URL https://doi.org/10.1017/CBO9781139059961

[17] A. Huber, W. Polifke, Dynamics of Practical Premixed Flames, Part I: Model Structure and Identification, International Journal of Spray and Combustion Dynamics 1 (2) (2009) 199–228. doi:10.1260/175682709788707431.
URL http://journals.sagepub.com/doi/10.1260/175682709788707431

[18] A. Huber, W. Polifke, Dynamics of Practical Premixed Flames, Part II: Identification and Interpretation of CFD Data, International Journal of Spray and Combustion Dynamics 1 (2) (2009) 229–249. doi:10.1260/175682709788707440.
URL http://journals.sagepub.com/doi/10.1260/175682709788707440

[19] C. O. Paschereit, W. Polifke, Investigation of the Thermoacoustic Characteristics of a Lean Premixed Gas Turbine Burner, in: Volume 3: Coal,

Biomass and Alternative Fuels; Combustion and Fuels; Oil and Gas Applications; Cycle Innovations, Paper No. 98-GT-582, ASME, Stockholm, Sweden, 1998. doi:10.1115/98-GT-582.
URL https://asmedigitalcollection.asme.org/GT/proceedings/GT1998/78644/Stockholm,%20Sweden/246907

[20] B. Schuermans, F. Guethe, D. Pennell, D. Guyot, C. O. Paschereit, Thermoacoustic Modeling of a Gas Turbine Using Transfer Functions Measured Under Full Engine Pressure, Journal of Engineering for Gas Turbines and Power 132 (11) (2010) 111503. doi:10.1115/1.4000854.
URL https://asmedigitalcollection.asme.org/gasturbinespower/article/doi/10.1115/1.4000854/464788/Thermoacoustic-Modeling-of-a-Gas-Turbine-Using

[21] L. Crocco, Theoretical studies on liquid-propellant rocket instability, Symposium (International) on Combustion 10 (1) (1965) 1101–1128. doi:10.1016/S0082-0784(65)80249-1.
URL https://linkinghub.elsevier.com/retrieve/pii/S0082078465802491

[22] Y. Yang, N. Noiray, A. Scarpato, O. Schulz, K. M. Düsing, M. Bothien, Numerical Analysis of the Dynamic Flame Response in Alstom Reheat Combustion Systems, in: Volume 4A: Combustion, Fuels and Emissions, Paper No. GT2015-42622, ASME, Montreal, Quebec, Canada, 2015. doi:10.1115/GT2015-42622.
URL http://proceedings.asmedigitalcollection.asme.org/proceeding.aspx?doi=10.1115/GT2015-42622

[23] A. Scarpato, L. Zander, R. Kulkarni, B. Schuermans, Identification of Multi-Parameter Flame Transfer Function for a Reheat Combustor, in: Volume 4B: Combustion, Fuels and Emissions, Paper No. GT2016-57699, ASME, Seoul, South Korea, 2016. doi:10.1115/GT2016-57699.

URL http://proceedings.asmedigitalcollection.asme.org/proceeding.aspx?doi=10.1115/GT2016-57699

[24] M. Bothien, D. Lauper, Y. Yang, A. Scarpato, Reconstruction and Analysis of the Acoustic Transfer Matrix of a Reheat Flame From Large-Eddy Simulations, Journal of Engineering for Gas Turbines and Power 141 (2) (2019) 021018. doi:10.1115/1.4041151.
URL https://asmedigitalcollection.asme.org/gasturbinespower/article/doi/10.1115/1.4041151/476200/Reconstruction-and-Analysis-of-the-Acoustic

[25] O. Schulz, N. Noiray, Autoignition flame dynamics in sequential combustors, Combustion and Flame 192 (2018) 86–100. doi:10.1016/j.combustflame.2018.01.046.
URL https://linkinghub.elsevier.com/retrieve/pii/S0010218018300609

[26] M. Poyyapakkam, J. Wood, S. Mayers, A. Ciani, F. Guethe, K. Syed, Hydrogen Combustion Within a Gas Turbine Reheat Combustor, in: Volume 2: Combustion, Fuels and Emissions, Parts A and B, Paper No. GT2012-69165, ASME, Copenhagen, Denmark, 2012, pp. 847–854. doi:10.1115/GT2012-69165.
URL https://asmedigitalcollection.asme.org/GT/proceedings/GT2012/44687/847/250462

[27] M. Brower, E. L. Petersen, W. Metcalfe, H. J. Curran, M. Füri, G. Bourque, N. Aluri, F. Güthe, Ignition Delay Time and Laminar Flame Speed Calculations for Natural Gas/Hydrogen Blends at Elevated Pressures, Journal of Engineering for Gas Turbines and Power 135 (2) (2013) 021504. doi:10.1115/1.4007763.
URL https://asmedigitalcollection.asme.org/gasturbinespower/article/doi/10.1115/1.4007763/373384/Ignition-Delay-Time-and-Laminar-Flame-Speed

[28] T. Wind, F. Güthe, K. Syed, Co-Firing of Hydrogen and Natural Gases in Lean Premixed Conventional and Reheat Burners (Alstom GT26), in: Volume 4A: Combustion, Fuels and Emissions, Paper No. GT2014-25813, ASME, Düsseldorf, Germany, 2014. doi:10.1115/GT2014-25813.
URL https://asmedigitalcollection.asme.org/GT/proceedings/GT2014/45684/D%C3%BCsseldorf,%20Germany/234996

[29] C. Xu, J.-W. Park, C. S. Yoo, J. H. Chen, T. Lu, Identification of premixed flame propagation modes using chemical explosive mode analysis, Proceedings of the Combustion Institute 37 (2) (2019) 2407–2415. doi:10.1016/j.proci.2018.07.069.
URL https://linkinghub.elsevier.com/retrieve/pii/S1540748918304875

[30] B. Savard, E. R. Hawkes, K. Aditya, H. Wang, J. H. Chen, Regimes of premixed turbulent spontaneous ignition and deflagration under gas-turbine reheat combustion conditions, Combustion and Flame 208 (2019) 402–419. doi:10.1016/j.combustflame.2019.07.020.
URL https://linkinghub.elsevier.com/retrieve/pii/S001021801930327X

[31] K. Aditya, A. Gruber, C. Xu, T. Lu, A. Krisman, M. R. Bothien, J. H. Chen, Direct numerical simulation of flame stabilization assisted by autoignition in a reheat gas turbine combustor, Proceedings of the Combustion Institute 37 (2) (2019) 2635–2642. doi:10.1016/j.proci.2018.06.084.
URL https://linkinghub.elsevier.com/retrieve/pii/S1540748918302670

[32] A. Ni, W. Polifke, F. Joos, Ignition Delay Time Modulation as a Contribution to Thermo-Acoustic Instability in Sequential Combustion, in: Volume 2: Coal, Biomass and Alternative Fuels; Combustion and Fuels; Oil and Gas Applications; Cycle Innovations, Paper No. 2000-GT-0103,

ASME, Munich, Germany, 2000. doi:10.1115/2000-GT-0103.
URL https://asmedigitalcollection.asme.org/GT/proceedings/GT2000/78552/Munich,%20Germany/245243

[33] M. Zellhuber, V. Bellucci, B. Schuermans, W. Polifke, Modelling the Impact of Acoustic Pressure Waves on Auto-Ignition Flame Dynamics, in: Proceedings of the European Combustion Meeting, FESCI, Cardiff, UK, 2011.

[34] J. Li, Z. Zhao, A. Kazakov, F. L. Dryer, An updated comprehensive kinetic model of hydrogen combustion, International Journal of Chemical Kinetics 36 (10) (2004) 566–575. doi:10.1002/kin.20026.
URL http://doi.wiley.com/10.1002/kin.20026

[35] Y. Jiang, G. d. Alamo, A. Gruber, M. R. Bothien, K. Seshadri, F. A. Williams, A skeletal mechanism for prediction of ignition delay times and laminar premixed flame velocities of hydrogen-methane mixtures under gas turbine conditions, International Journal of Hydrogen Energy 44 (33) (2019) 18573–18585. doi:10.1016/j.ijhydene.2019.05.068.
URL https://linkinghub.elsevier.com/retrieve/pii/S036031991931924X

[36] J. H. Chen, A. Choudhary, B. de Supinski, M. DeVries, E. R. Hawkes, S. Klasky, W. K. Liao, K. L. Ma, J. Mellor-Crummey, N. Podhorszki, R. Sankaran, S. Shende, C. S. Yoo, Terascale direct numerical simulations of turbulent combustion using S3D, Computational Science & Discovery 2 (1) (2009) 015001. doi:10.1088/1749-4699/2/1/015001.
URL https://iopscience.iop.org/article/10.1088/1749-4699/2/1/015001

[37] C. A. Kennedy, M. H. Carpenter, R. Lewis, Low-storage, explicit Runge–Kutta schemes for the compressible Navier–Stokes equations, Applied Numerical Mathematics 35 (3) (2000) 177–219. doi:10.1016/S0168-9274(99)00141-5.

URL https://linkinghub.elsevier.com/retrieve/pii/S0168927499001415

[38] T. Poinsot, S. Lele, Boundary conditions for direct simulations of compressible viscous flows, Journal of Computational Physics 101 (1) (1992) 104–129. doi:10.1016/0021-9991(92)90046-2.
URL https://linkinghub.elsevier.com/retrieve/pii/0021999192900462

[39] J. C. Sutherland, C. A. Kennedy, Improved boundary conditions for viscous, reacting, compressible flows, Journal of Computational Physics 191 (2) (2003) 502–524. doi:10.1016/S0021-9991(03)00328-0.
URL https://linkinghub.elsevier.com/retrieve/pii/S0021999103003280

[40] F. Gant, A. Scarpato, M. R. Bothien, Occurrence of multiple flame fronts in reheat combustors, Combustion and Flame 205 (2019) 220–230. doi:10.1016/j.combustflame.2019.04.013.
URL https://linkinghub.elsevier.com/retrieve/pii/S0010218019301580

[41] R. Kulkarni, M. Zellhuber, W. Polifke, LES based investigation of autoignition in turbulent co-flow configurations, Combustion Theory and Modelling 17 (2) (2013) 224–259. doi:10.1080/13647830.2012.739711.
URL http://www.tandfonline.com/doi/abs/10.1080/13647830.2012.739711

[42] R. Kulkarni, B. Bunkute, F. Biagioli, M. Duesing, W. Polifke, Large Eddy Simulation of ALSTOM's Reheat Combustor Using Tabulated Chemistry and Stochastic Fields-Combustion Model, in: Volume 4B: Combustion, Fuels and Emission, Paper No. GT2014-26053, ASME, Düsseldorf, Germany, 2014. doi:10.1115/GT2014-26053.
URL https://asmedigitalcollection.asme.org/GT/proceedings/GT2014/45691/D%C3%BCsseldorf,%20Germany/235030

This is the accepted version of an article pulished in Combustion and Flame
http://dx.doi.org/10.1016/j.combustflame.2020.09.005

[43] R. Kulkarni, Large Eddy Simulation of Autoignition in Turbulent Flows, Ph.D. thesis, Technische Universität München, Munich, Germany (2013).

[44] A. S. Morgans, I. Duran, Entropy noise: A review of theory, progress and challenges, International Journal of Spray and Combustion Dynamics 8 (4) (2016) 285–298. doi:10.1177/1756827716651791.
URL http://journals.sagepub.com/doi/10.1177/1756827716651791

[45] F. Marble, S. Candel, Acoustic disturbance from gas non-uniformities convected through a nozzle, Journal of Sound and Vibration 55 (2) (1977) 225–243. doi:10.1016/0022-460X(77)90596-X.
URL https://linkinghub.elsevier.com/retrieve/pii/0022460X7790596X

[46] L. Magri, On indirect noise in multicomponent nozzle flows, Journal of Fluid Mechanics 828 (2017). doi:10.1017/jfm.2017.591.
URL https://www.cambridge.org/core/product/identifier/S0022112017005912/type/journal_article

[47] F. Bake, N. Kings, I. Roehle, Fundamental Mechanism of Entropy Noise in Aero-Engines: Experimental Investigation, Journal of Engineering for Gas Turbines and Power 130 (1) (2008) 011202. doi:10.1115/1.2749286.
URL https://asmedigitalcollection.asme.org/gasturbinespower/article/doi/10.1115/1.2749286/470332/Fundamental-Mechanism-of-Entropy-Noise-in

[48] W. C. Strahle, Combustion noise, Progress in Energy and Combustion Science 4 (3) (1978) 157–176. doi:10.1016/0360-1285(78)90002-3.
URL https://linkinghub.elsevier.com/retrieve/pii/0360128578900023

[49] M. Ihme, Combustion and Engine-Core Noise, Annual Review of Fluid Mechanics 49 (1) (2017) 277–310. doi:10.1146/annurev-fluid-122414-034542.

URL http://www.annualreviews.org/doi/10.1146/annurev-fluid-122414-034542

[50] O. Schulz, U. Doll, D. Ebi, J. Droujko, C. Bourquard, N. Noiray, Thermoacoustic instability in a sequential combustor: Large eddy simulation and experiments, Proceedings of the Combustion Institute 37 (4) (2019) 5325–5332. doi:10.1016/j.proci.2018.07.089.
URL https://linkinghub.elsevier.com/retrieve/pii/S1540748918305078

[51] A. Giusti, N. A. Worth, E. Mastorakos, A. P. Dowling, Experimental and Numerical Investigation into the Propagation of Entropy Waves, AIAA Journal 55 (2) (2017) 446–458. doi:10.2514/1.J055199.
URL https://arc.aiaa.org/doi/10.2514/1.J055199

[52] M. Zellhuber, L. Tay Wo Chong, W. Polifke, Non-Linear Flame Response at Small Perturbation Amplitudes - Consequences for Analysis of Thermoacoustic Instabilities, in: Proceedings of the European Combustion Meeting, FESCI, Cardiff, UK, 2011.

[53] W. Polifke, A. Poncet, C. Paschereit, K. Döbbeling, Reconstruction of acoustic transfer matrices by instationary computational fluid dynamics, Journal of Sound and Vibration 245 (3) (2001) 483–510. doi:10.1006/jsvi.2001.3594.
URL https://linkinghub.elsevier.com/retrieve/pii/S0022460X01935941

[54] B. Ćosić, S. Terhaar, J. P. Moeck, C. O. Paschereit, Response of a swirl-stabilized flame to simultaneous perturbations in equivalence ratio and velocity at high oscillation amplitudes, Combustion and Flame 162 (4) (2015) 1046–1062. doi:10.1016/j.combustflame.2014.09.025.
URL https://linkinghub.elsevier.com/retrieve/pii/S001021801400306X

This is the accepted version of an article publised in Combustion and Flame
http://dx.doi.org/10.1016/j.combustflame.2020.09.005

[55] N. Noiray, D. Durox, T. Schuller, S. Candel, A unified framework for nonlinear combustion instability analysis based on the flame describing function, Journal of Fluid Mechanics 615 (2008) 139–167. doi:10.1017/S0022112008003613.
URL https://www.cambridge.org/core/product/identifier/S0022112008003613/type/journal_article

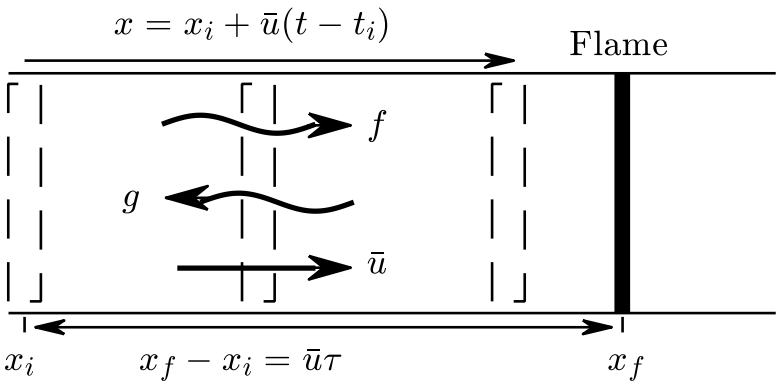

Figure 1: Sketch of the model setup.

This is the accepted version of an article publised in Combustion and Flame
http://dx.doi.org/10.1016/j.combustflame.2020.09.005

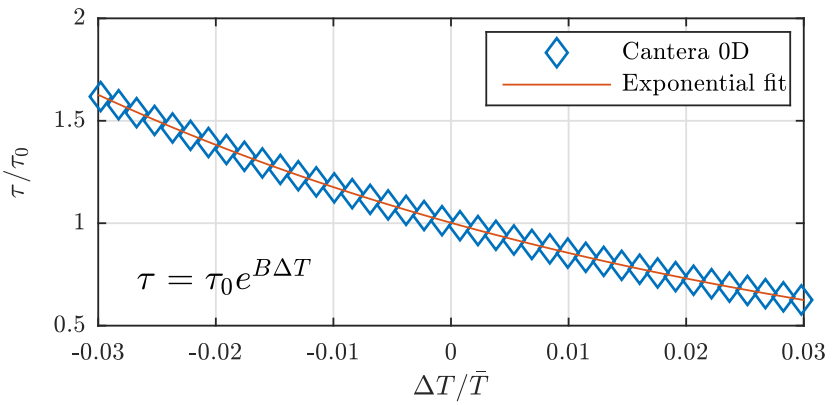

Figure 2: Ignition delay time of a homogeneous mixture of air and methane for different temperatures. Results obtained from 0-dimensional Cantera simulations.

This is the accepted version of an article publised in Combustion and Flame
http://dx.doi.org/10.1016/j.combustflame.2020.09.005

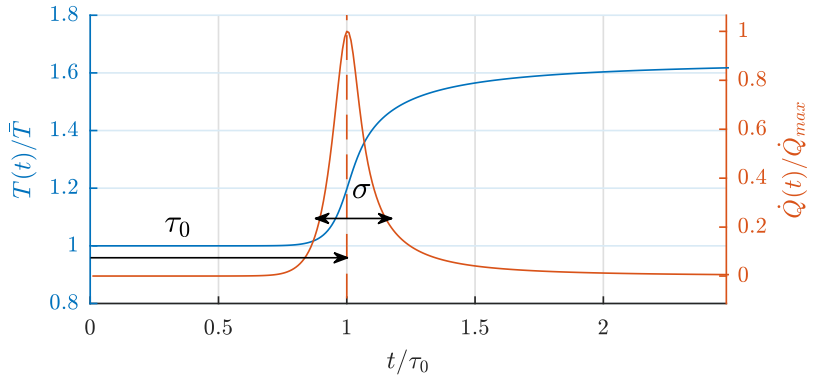

Figure 3: Temperature and heat release rate profile over time. Results obtained from 0-dimensional Cantera simulations.

This is the accepted version of an article publised in Combustion and Flame
http://dx.doi.org/10.1016/j.combustflame.2020.09.005

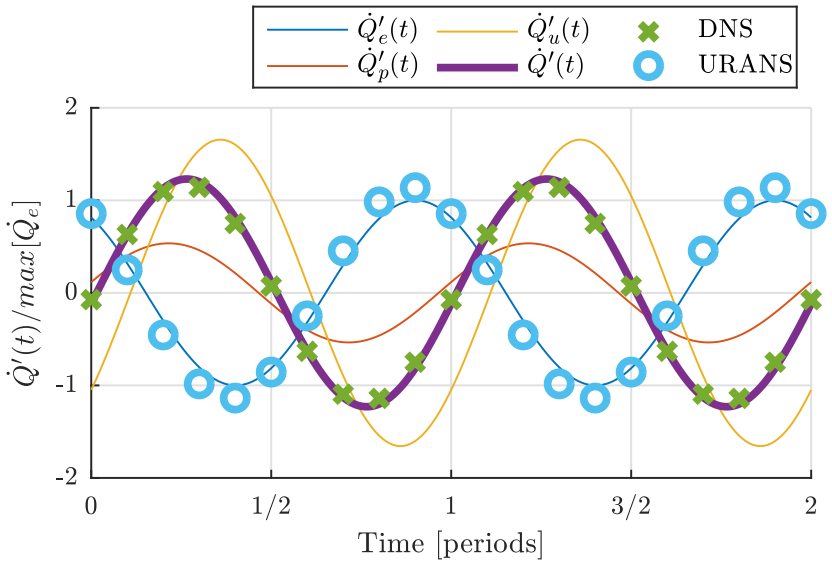

Figure 4: Two periods of unsteady normalized heat release rate, hydrogen flame forced at 100 Hz with 2 K. DNS and URANS (symbols) are compared to the 3 terms on the right hand side of Eq. (12) and their sum (purple curve).

This is the accepted version of an article publised in Combustion and Flame
http://dx.doi.org/10.1016/j.combustflame.2020.09.005

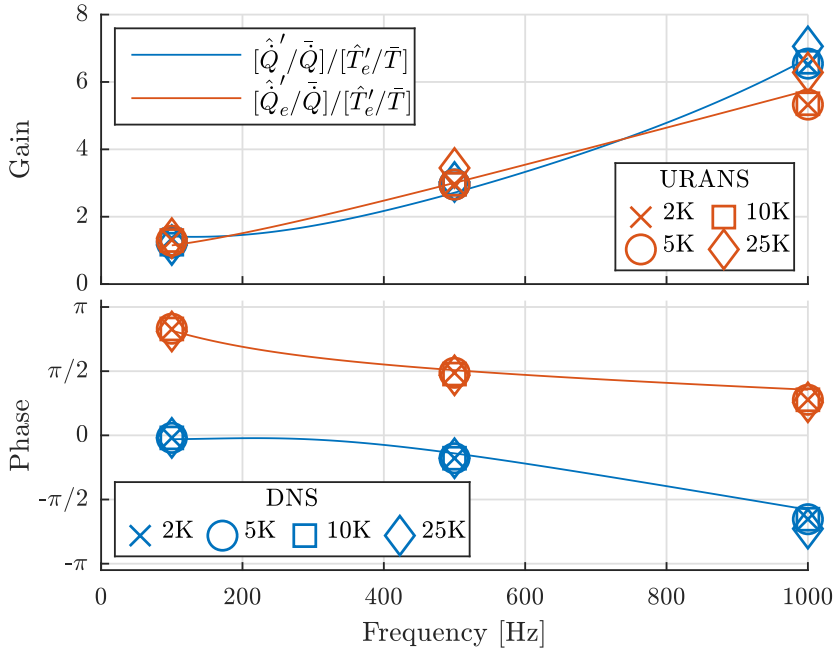

Figure 5: $\hat{\dot{Q}}'/\bar{\dot{Q}}$ normalized by $\hat{T}'_e/\bar{T}$; results extracted over the 2 sets of 12 DNS and URANS simulations. Blue line: analytical expression for $\hat{\dot{Q}}'/\bar{\dot{Q}}$ in Eq. (12). Red line: entropic part $\hat{\dot{Q}}'_e/\bar{\dot{Q}}$, first term on the right hand side of Eq. (12). The fuel is hydrogen.

This is the accepted version of an article publised in Combustion and Flame
http://dx.doi.org/10.1016/j.combustflame.2020.09.005

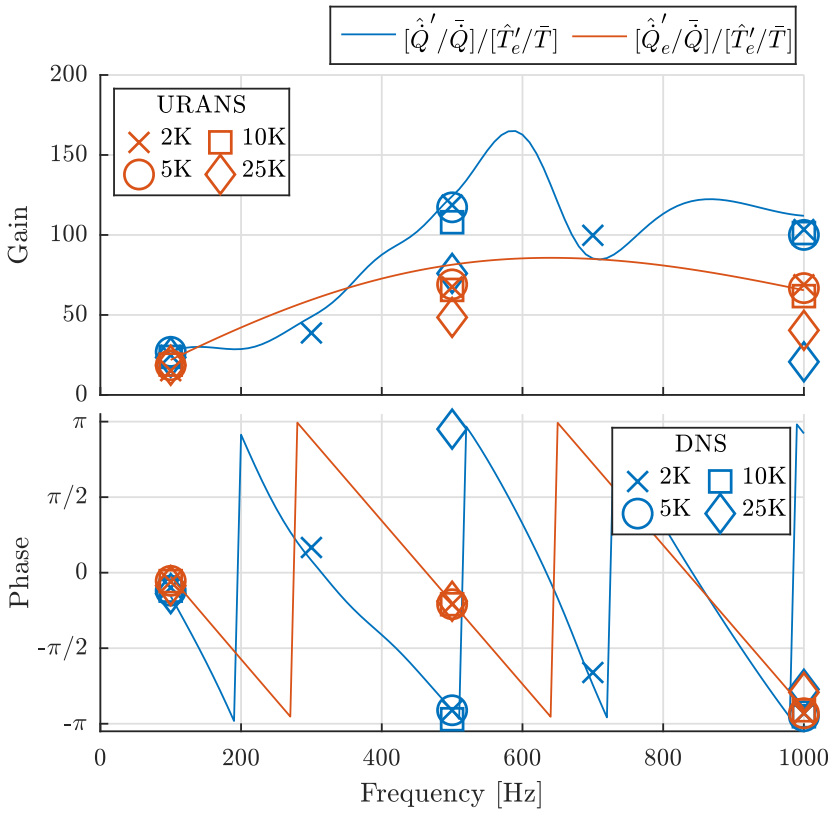

Figure 6: $\hat{\dot{Q}}'/\bar{\dot{Q}}$ normalized by $\hat{T}'_e/\bar{T}$; results extracted over the 2 sets of 12 DNS and URANS simulations. Blue line: analytical expression for $\hat{\dot{Q}}'/\bar{\dot{Q}}$ in Eq. (12). Red line: entropic part $\hat{\dot{Q}}'_e/\bar{\dot{Q}}$, first term on the right hand side of Eq. (12). The fuel is methane. Two additional DNS simulations at $f = 300\,\mathrm{Hz}$ and $f = 700\,\mathrm{Hz}$ and $\Delta T = 2\,\mathrm{K}$ are reported.

This is the accepted version of an article publised in Combustion and Flame
http://dx.doi.org/10.1016/j.combustflame.2020.09.005

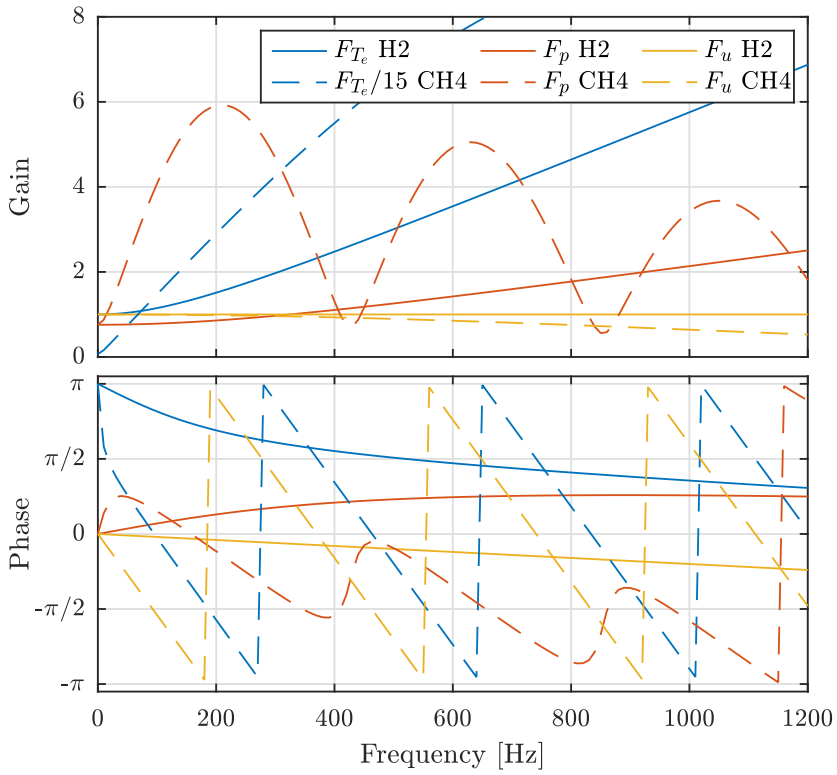

Figure 7: Entropic and acoustic flame transfer functions (gain and phase) versus frequency from right hand side of Eq. (12), for both the hydrogen and methane case. The gain of the entropy transfer function F_{T_e} has been divided by 15 in the methane case.

This is the accepted version of an article publised in Combustion and Flame
http://dx.doi.org/10.1016/j.combustflame.2020.09.005

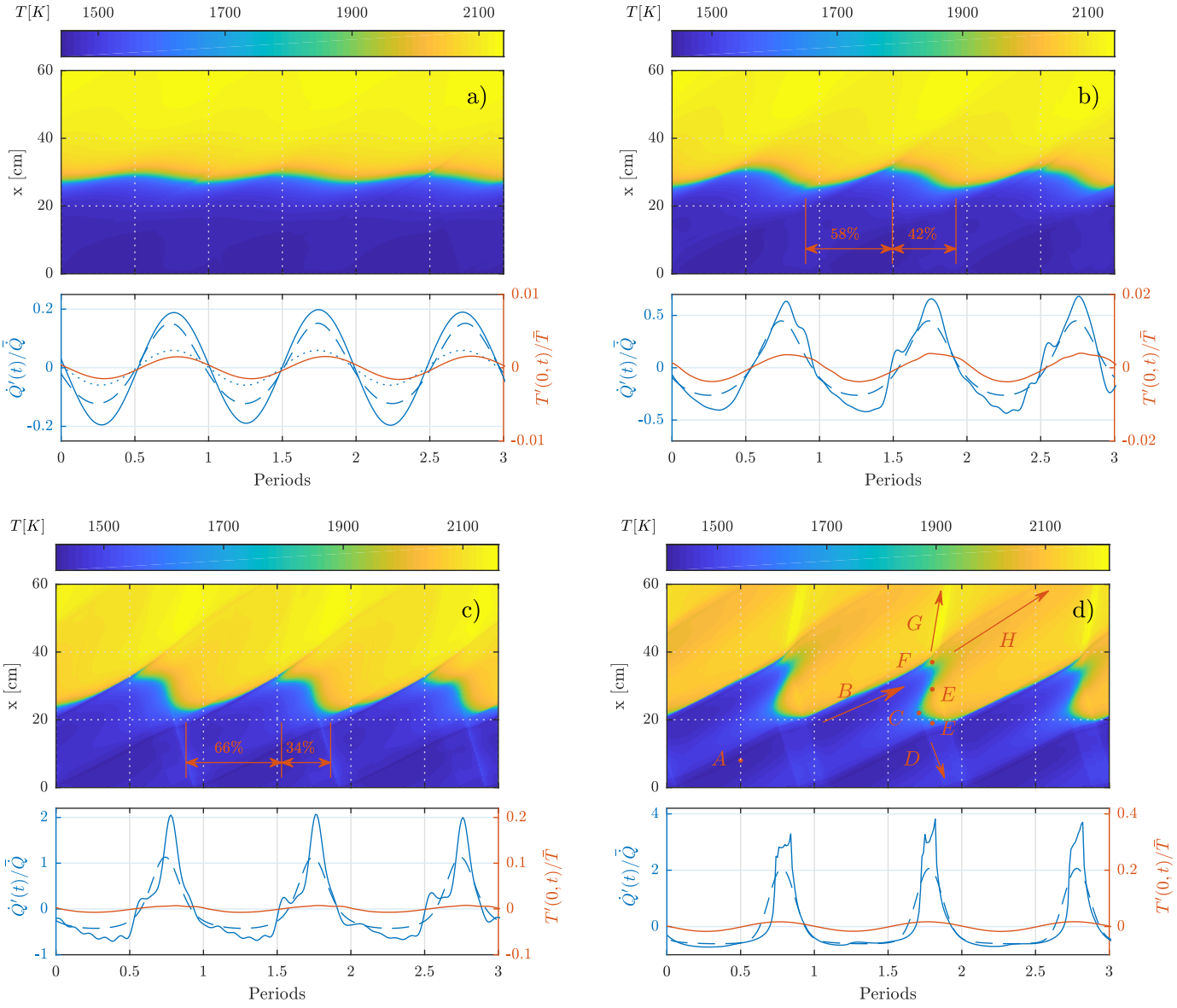

Figure 8: DNS simulations of methane flames excited at $f = 500\,\mathrm{Hz}$ with $\Delta T = 2$ (a), 5 (b), 10 (c) and 25 K (d), respectively. Top (in each frame): temperature field over time (in periods of inlet excitation) and space (in cm). Bottom (in each frame): spatially-integrated normalized heat release rate $\dot{Q}'(t)/\bar{\dot{Q}}$ over time (continuous blue line), analytical $\dot{Q}'_e(t)/\bar{\dot{Q}}$ from numerical integration of Eq. (8) (dashed blue line), analytical $\dot{Q}'_a(t)/\bar{\dot{Q}}$ from Eq. (10) (dotted blue line), normalized inlet temperature forcing $T'(x=0,t)/\bar{T}$ (continuous red line).

This is the accepted version of an article published in Combustion and Flame
http://dx.doi.org/10.1016/j.combustflame.2020.09.005

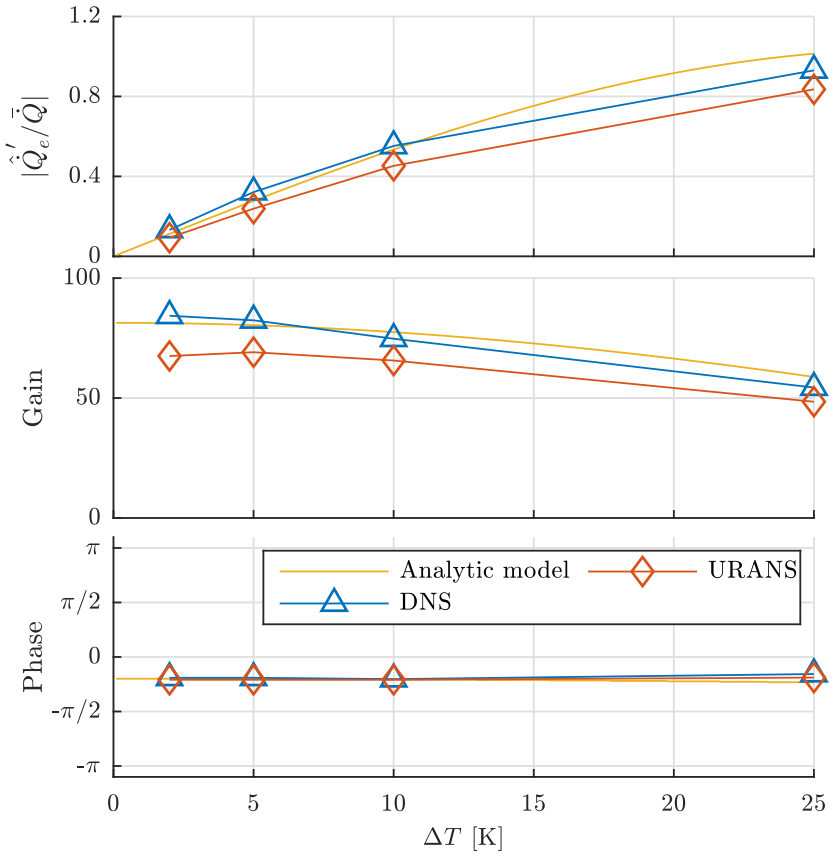

Figure 9: Top plot: amplitude of the entropic part of normalized heat release rate, $|\hat{\dot{Q}}_e'/\bar{\dot{Q}}|$. Middle and bottom plots: gain and phase of $[\hat{\dot{Q}}_e'/\bar{\dot{Q}}]/[\hat{T}_e'/\bar{T}]$ respectively.

This is the accepted version of an article publised in Combustion and Flame
http://dx.doi.org/10.1016/j.combustflame.2020.09.005

This is the accepted version of an article publised in Combustion and Flame
http://dx.doi.org/10.1016/j.combustflame.2020.09.005

Declaration of interests

☒ The authors declare that they have no known competing financial interests or personal relationships that could have appeared to influence the work reported in this paper.

☐The authors declare the following financial interests/personal relationships which may be considered as potential competing interests:

This is the accepted version of an article publised in Combustion and Flame
http://dx.doi.org/10.1016/j.combustflame.2020.09.005